*Solar RRL*

WILEY VCH

Solar RRL

PERSPECTIVE OPEN ACCESS

# Heuristic Rule of Thumb for Tandem Solar Cells and Perspectives for the Future

Martina Schmid

Faculty of Physics and CENIDE, University of Duisburg-Essen, Duisburg, Germany

**Correspondence:** Martina Schmid (martina.schmid@uni-due.de)

**Received:** 24 January 2025 | **Revised:** 27 March 2025 | **Accepted:** 31 March 2025

**Funding:** Open Access Publication Fund of the University of Duisburg-Essen

**Keywords:** bifacial tandem solar cell | current matching | future tandem configuration | minimum efficiency requirement | spectrum-splitting concentrator | tandem solar cell | top cell transparency

## ABSTRACT

Photovoltaics has gained significant interest as renewable electricity source. For cost reduction, maximizing efficiency is paramount. Tandem solar cells, combining two absorbers with different band gaps, offer improved solar spectrum utilization. Hereby, a two-terminal configuration simplifies the layer structure but demands current matching. While the search for new, especially top absorber materials continues, we focus on fundamental tandem solar cell principles to emphasize key requirements. We analyze how top-cell transparency affects bottom-cell performance in stacked tandems. Imperfect transmission impacts the bottom cell, but in a current-matched device, even the top-cell efficiency. To match the bottom-cell performance, 50% top-cell transmission and 50% efficiency relative to the single bottom cell are required, but higher values to surpass it. Subgap transparency remains a critical challenge, underscoring the need for top-cell efficiencies approaching those of the bottom cell. To relax particularly current-matching constraints, concepts like luminescent coupling, wavelength-selective intermediate reflectors, or bifacial illumination may be considered. Operating under light concentration further enhances efficiency and better justifies tandem fabrication costs. Looking ahead, bifacial tandem concentrator cells, in a three-terminal configuration and combined with spectrum-splitting optics to reduce optical losses and improve adaptability to variable illumination, offer an innovative pathway.

## 1 | Introduction

The thrive for higher efficiencies is driving photovoltaic research. Numerous strategies have been explored to surpass the Shockley–Queisser efficiency limit for single-junction solar cells. Tandem or multijunction solar cells are to date the only proven designs achieving efficiencies beyond 30% under one-sun illumination. Unlike single-junction solar cells, which can fully convert only photons with energies matching their bandgap $E_g$ into electricity, the combination of different absorber materials in tandem designs enables more effective utilization of the incident solar spectrum. The limiting factors are visualized in the inset in Figure 1 [1]: Photons with energies below the bandgap do not generate electron–hole pairs, while those with energies above the bandgap lose their excess energy through thermalization. The main Figure 1 emphasizes these constraints for a solar cell having $E_g = 1.1$ eV where the photon energy is only fully exploited for 1.1 eV and the usage reduces for higher energies (red area). By introducing a second solar cell with here $E_g = 1.7$ eV on top, also the photons with 1.7 eV energy are fully utilized, while higher-energy photons are more effectively converted (blue area). The improvement is visible as the light blue area in the figure, complementing the dark region that represents the original bottom-cell contribution (shown in red beneath).

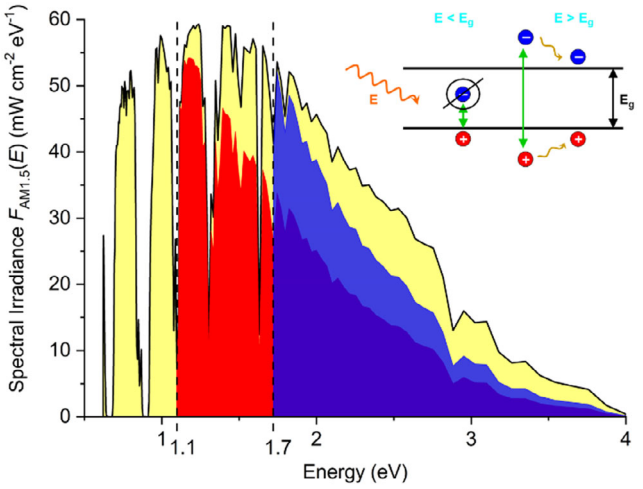


**FIGURE 1** | Solar irradiation (AM1.5 spectrum, yellow) utilized by a solar cell with $E_g = 1.1$ eV (red) and $E_g = 1.7$ eV (blue, overlapped), respectively. Background shown in inset: Photons with below-bandgap energy remain unabsorbed; higher energetic ones thermalize to the band edges (adapted from own data [1]).

The usable irradiance $g$ can be described mathematically by

$$g(E_g) = \int_{E_g}^{\infty} F_{AM1.5}(E) \cdot \frac{E_g}{E} dE = \dot{n}_{ph} \cdot E_g \quad (1)$$

where $F_{AM1.5}(E)$ is the spectral irradiance and $\dot{n}_{ph}$ the photon flux density. Hereby, the lower integration limit, $E_g$, accounts for the nonutilization of photons with energies $E < E_g$, while the factor $E_g/E$ within the integral reflects the thermal losses during charge separation by photons with energies $E > E_g$.

Comprehensive research has explored the maximum efficiencies and optimal bandgap combinations for multijunction solar cells. Using the detailed balance framework, upper-efficiency limits were calculated under idealized conditions, assuming perfect spectral splitting between the top and bottom cell [2]. Following early literature [3], tandem efficiencies as a function of the top- and bottom-cell bandgap have been mapped in numerous publications, generally neglecting parasitic absorption in the top cell. Although this absorption significantly affects performance, it has so far received less attention [4–6]. More recent studies have emphasized cost considerations to make tandem cells economically viable [7, 8]. This work focuses on the critical yet often overlooked role of top-cell transparency in tandem performance, encompassing the requirements for the initial efficiency of the top cell and its performance degradation in current-matched devices.

## 2 | Fundamental Tandem Considerations

Achieving high tandem efficiencies requires two essential ingredients. First is the intrinsic efficiency of the two subcells, a factor that has been extensively studied and discussed in most publications. Second, and often overlooked, is the transparency of the top cell. Here, we are not just talking about the spectrum-cutting occurring due to the nature of the tandem configuration. It is rather the incomplete subgap transmission that tips the balance and deserves at least equal attention as we will show below. Subgap transmission is not solely a matter of the absorber, but of all the layers building up the solar cell. In this context, the configuration of the tandem plays a central role.

Figure 2 shows the basic configurations of tandem solar cells with four, three, or two terminals (4T, 3T, and 2T). The simplest configuration involves electrically independent top and bottom cells, resulting in four total connections (4T, Figure 2a). These cells are stacked optically and possibly mechanically, without direct electrical coupling. This design offers significant advantages, such as the ability to fabricate the top and bottom cells separately, which is particularly useful in cases where high-temperature processes must be paired with temperature-sensitive layers. Additionally, the two cells operate independently at their respective maximum power points, eliminating concerns about junction alignment or variations in performance due to changing irradiation conditions. However, this configuration suffers from high parasitic losses, as it requires full contact layers and thicknesses to enable lateral charge carrier extraction. To address the limitations of thick contacts while preserving electrical flexibility, 3T tandems were designed by connecting the bottom contact of the top cell to the top contact of the bottom cell. A third terminal was introduced either between these connections (as shown in Figure 2b) or through the double-interdigitated back contact of the bottom cell [9]. These diverse configurations highlight the adaptability of the approach while also necessitating a refined and sophisticated electrical design. The electric conditions are much more straightforward in the classical 2T tandem where top and bottom cell are, generally monolithically, series connected (Figure 2c). The pn-junctions of the two cells must be

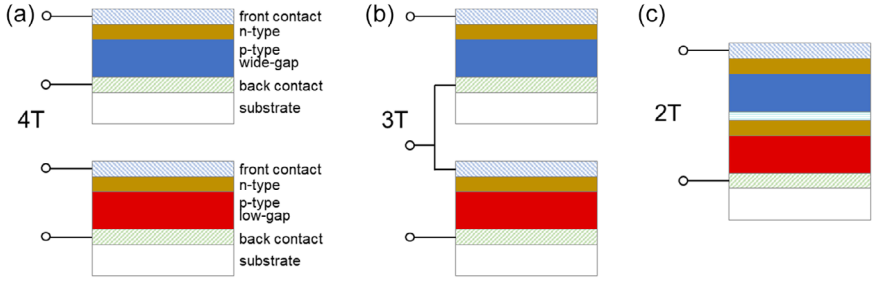


**FIGURE 2** | Basic tandem configurations with (a) four terminals, (b) three terminals and (c) two terminals. Exemplary np-junctions are shown as well as common configurations of separate substrates (4T), interconnected intermediate contacts (3T), and monolithic integration with tunneling junction (2T).

aligned so that the current can flow directly between them, often facilitated by a tunnel junction. This configuration reduces the number and thickness of intermediate layers, thereby minimizing parasitic optical absorption and maximizing light utilization. However, this design requires current matching between the top and bottom cell, meaning that the device's overall performance is constrained by the cell with the lower current output.

The maximum photocurrent density $j_{ph}$ of a solar cell can be derived from the photon flux density (Equation (1)) by setting the integration ranges corresponding to the band gap energies (i.e., top cell from $E_{g,\,top}$ to infinity and bottom cell from $E_{g,\,bottom}$ to $E_{g,\,top}$). Furthermore, since we will subsequently consider top-cell transparency, which is typically measured as a function of wavelength, we transition to the wavelength-dependent formulation. Asuming that each photon may generate at maximum one electron–hole-pair we have

$$j_{ph} = e \cdot \dot{n}_{ph} \tag{2}$$

with $e$ the elementary charge.

In a 2T tandem, the common current $j_{tandem}$ through the tandem structure is given by

$$j_{tandem} = \min\left(j_{top,single}, j_{bottom,shaded}\right) \tag{3}$$

where

$$\begin{aligned} j_{bottom,\,shaded} &= e \cdot \int_{\lambda_{g,bottom}}^{\infty} T_{top}(\lambda) \cdot F_{AM1.5}(\lambda) \cdot \frac{\lambda}{h \cdot c} d\lambda \\ &\approx j_{bottom,single} \cdot T_{top} \end{aligned} \tag{4}$$

with $\lambda_g$ the bandgap wavelength, h Planck's constant, and c the speed of light. $T_{top}(\lambda)$ is the wavelength-dependent top-cell transparency, while $T_{top}$ is the average one. In reality, the integration limit infinity needs to be replaced by the bandgap wavelength of the front contact layers. The crucial point here is the top-cell transparency. The current-matching condition of top and bottom cell, which was fulfilled for the optimum band gap combination, may no longer hold due to parasitic absorption losses. Adjustment is needed which is feasible by adjusting the bandgaps or the top absorber thickness. Essentially, a low transparency of the top cell not just deteriorates the bottom-cell performance but, due to the current-matching constraints, also compromises its own (details following below). Thus, the top cell's subgap transparency is one if not the most important criteria determining the tandem performance and thus deserves substantial consideration.

In addition to its transparency, we need to look at the top-cell efficiency. Since the total tandem efficiency $\eta_{tandem} = \eta_{top,tandem} + \eta_{bottom,tandem}$, we need to request

$$\eta_{top,\,tandem} > \eta_{bottom,\,single} - \eta_{bottom,\,tandem} \tag{5}$$

to make the tandem perform superior to the single (bottom) cell.

In the following, let us assume that the bottom-cell current in the tandem configuration is the limiting factor, that is, $j_{tandem} = j_{bottom,shaded}$. By just considering the impact of changed $j_{bottom,tandem}$, but not its implication on other photovoltaic parameters, we can estimate

$$\eta_{bottom,tandem} \approx \eta_{bottom,single} \cdot T_{top} \tag{6}$$

In principle, changes in $j_{sc}$ may also affect other solar cell parameters. In particular, the open-circuit voltage $V_{oc}$ follows the variations of $j_{sc}$ according to the simplified diode equation: $V_{oc}' = V_{oc} + nkT/e \cdot \ln\left(j_{sc}'/j_{sc}\right)$ where the primed variables represent the modified values, $n$ is the diode quality factor, k the Boltzmann constant, and $T$ is the absolute temperature here. However, due to the logarithmic dependence, this effect is of secondary importance, and for simplicity, we focus primarily on the dominant influence of changing $j_{sc}$.

Subsequently,

$$\eta_{top,tandem} = \eta_{top,single} \cdot \frac{j_{tandem}}{j_{top,single}} = \eta_{top,single} \cdot \frac{j_{bottom,single}}{j_{top,single}} \cdot T_{top} \tag{7}$$

This equation explicitly shows the dependence of the top-cell performance in the tandem on its own transparency. Furthermore, we can combine Equation (5) and (6) to clarify the requirements for the top-cell efficiency (which can only decrease in the tandem, i.e., $\eta_{top,single} \geq \eta_{top,tandem}$)

$$\begin{aligned} \boldsymbol{\eta_{top,single}} &> \eta_{bottom,single}\left(1 - \frac{j_{tandem}}{j_{bottom,single}}\right) \\ &\approx \boldsymbol{\eta_{bottom,single}\left(1 - T_{top}\right)} \end{aligned} \tag{8}$$

Importantly, $T_{top}$ represents the equally averaged total transmission of the top cell, indicated by the $\approx$ sign to reflect an approximation. This transmission can never reach 100%, as complete transparency would mean no absorption occurs in the top absorber. Thus, the top cell inherently absorbs light above its bandgap and must compensate for subgap transmission losses with higher efficiency. Assuming an equal distribution of spectral irradiance between the two subcells in a balanced tandem, the average top-cell transparency is typically set at ≈50%. Under the rigorous assumption that the average transmittance will directly translate to changes in the bottom-cell photocurrent, a tandem solar cell can only surpass the single bottom-cell performance if the top cell achieves at least 50% of the bottom-cell efficiency. Importantly, any subgap absorption in the top cell necessitates additional compensation by increased efficiency. For instance, if the subgap transparency of the top cell is only 60% (rather than 100%), 40% of the light in this spectral range is lost, reducing the average top-cell transparency to approximately 30%. Under such conditions, the single top cell must achieve 70% of the bottom-cell efficiency instead of just 50%.

Figure 3a illustrates these observations from Equation (8) by showing the ratio of the single top-cell efficiency to the single bottom-cell efficiency as a function of the average top-cell transparency. The dark green line represents the scenario where the tandem performance equals that of the single bottom cell,

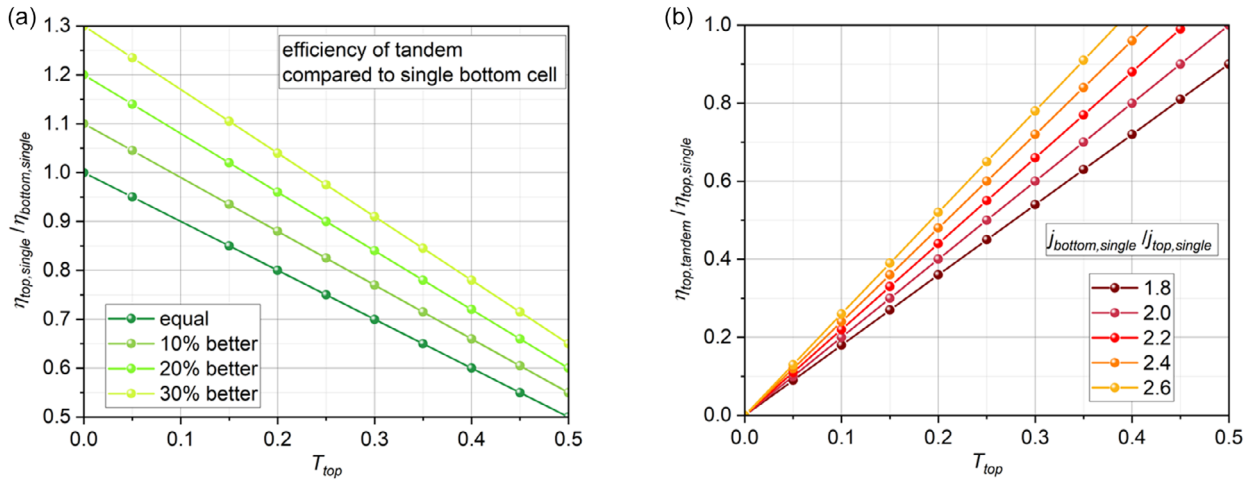


**FIGURE 3** | Visualization of (a) Equation (8) and (b) Equation (7), illustrating the influence of top-cell transparency on the initial efficiency requirements of the top cell and its degradation in a bottom-limited tandem, respectively.

indicating no net efficiency gain. This occurs for example when the top-cell transparency is 50%, and the single top-cell efficiency is 50% of the single bottom-cell efficiency. As top-cell transparency decreases, it must be offset by a higher initial top-cell efficiency—for example, an efficiency ratio of 80% is required for 20% top-cell transmission, just not to lose efficiency. The increasingly bright green lines provide guidance on how to obtain an improvement of 10%, 20%, or 30%. For instance, achieving a 30% higher tandem efficiency compared to the bottom cell alone requires a top cell with an initial efficiency that is 85% of the single bottom-cell efficiency if it offers an average transparency of only 35%.

Figure 3b further shows the consequences of current match in a 2T tandem according to Equation (7). The efficiency ratio of the top cell in the tandem over the single device is plotted against the average top-cell transparency for different current ratios of the single bottom over top cell. Based on the spectral irradiance division between the two cells, this latter ratio is typically around 2, meaning the photo-current density of the single bottom cell is approximately twice that of the single top cell and is expected to be halved by top-cell shading. If the current ratio falls below 2, a top-cell transparency of 50% is insufficient to maintain the top-cell efficiency in the tandem. In the example of a current ratio of 1.8 (darkest line), a top cell with 40% transparency retains only 80% of its initial efficiency. Thus, for transparencies below 50%, the top-cell efficiency risks degradation unless the initial bottom-to-top-cell current ratio exceeds 2. This compensation is illustrated by the yellow, orange, and red lines, which can maintain an efficiency ratio of 1 for top-cell transparencies below 50%. Note that the derivation of Equation (7) assumes a bottom-cell-limited 2T tandem (i.e., $j_{top,single} > j_{tandem} = j_{bottom,shaded}$).

Considering 3T or 4T tandem devices, where current matching is not required, the design constraints are relaxed. In these configurations, the minimum current is no longer enforced for both subcells, that is, Equation (3) does not hold. Specifically, $j_{top,tandem} = j_{top,single}$ can be maintained. However, $j_{bottom,tandem} = j_{bottom,shaded}$ will still be affected by shading from the top cell. As a result, poor transparency in the top cell deteriorates the bottom-cell performance. Although low top-cell transparency no longer impacts its own performance, it can still limit the overall tandem efficiency if the bottom-cell underperforms. Since Equations (4)–(6) remain applicable, Equation (8) also holds for 3T and 4T devices with $j_{tandem}$ replaced by $j_{bottom,tandem}$. Therefore, the considerations outlined in the previous paragraph regarding the minimum efficiency requirements for the top cell remain valid, as does the analysis presented in Figure 3a.

## 3 | Exemplary TopCell Transparencies and Impact

In practice, top-cell transparency exhibits a spectral dependence, which can be quantitatively analyzed based on spectral efficiency, as outlined by Yu et al. [10]. Despite this complexity, using an average top-cell transparency can still provide meaningful tandem performance predictions. To illustrate this, exemplary transparency values for various absorber materials are presented. Literature data for common material classes are shown in Figure 4. First, Figure 4a juxtaposes a prominent perovskite ($Cs_{0.09}FA_{0.77}MA_{0.14}Pb$ $(I_{0.86}Br_{0.14})_3$ [11]) to a wide-gap chalcopyrite ($Cu(In,Ga)S_2$ [12]) solar cell. Despite their thin absorber layers (500–600 nm), both materials exhibit nearly complete absorption above their bandgaps (<≈750 nm wavelength). However, their sub-bandgap transmission is incomplete averaging around 90% for the perovskite and around 65% for the chalcopyrite. Although these estimates are rough, they offer direct insights into the required top-cell efficiency and the potential to surpass single bottom-cell performance, as described by Equation (8).

In the example of $Cu(In,Ga)S_2$ [12], the single top cell achieved a short-circuit current density $j_{top,single}$ = 18.6 mA/cm$^2$ and an efficiency $\eta_{top,single}$ = 8.8%. In a stacked configuration with a $Cu(In,Ga)Se_2$ bottom cell, the bottom cell's performance declined from $j_{bottom,single}$ = 34.8 mA/cm$^2$ and $\eta_{bottom,single}$ = 17.7% to $j_{bottom,tandem}$ = 9.0 mA/cm$^2$ and $\eta_{bottom,tandem}$ = 4.6% due to the shading by the top cell. The subsequent current limitation of the 2T current-matched device to $j_{tandem}$ = 9.0 mA/cm$^2$ also

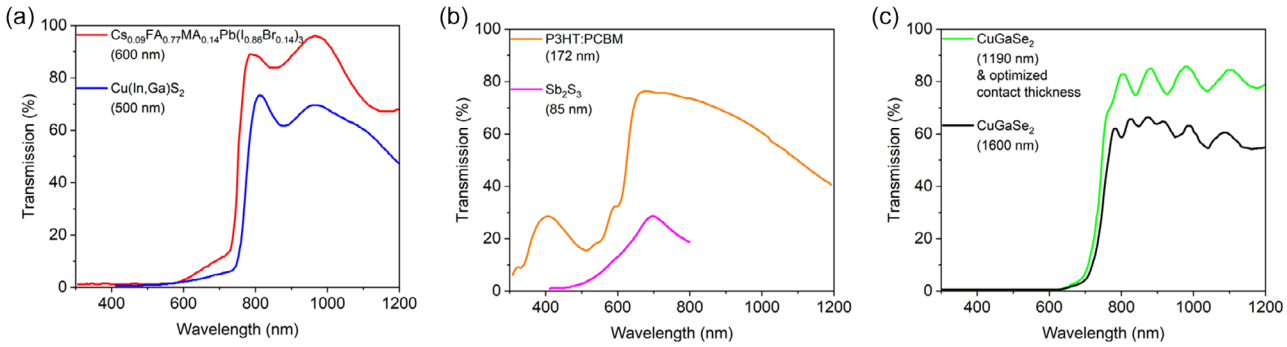


**FIGURE 4** | Transmission of semitransparent solar cells based on the indicated absorber materials and thicknesses as given in the respective references: (a) $Cs_{0.09}FA_{0.77}MA_{0.14}Pb\ (I_{0.86}Br_{0.14})_3$ (data from Ref. [11]) and $Cu(In,Ga)S_2$ (data from Ref. [12]), (b) P3HT:PCBM (data from Ref. [13]) and $Sb_2S_3$ (data from Ref. [14]), and (c) $CuGaSe_2$ (data from Ref. [15]). Details of the full device stacks can be found in the references.

constrained the top cell's performance (see Equation (7)), leading to a tandem efficiency of $\eta_{tandem} = 9.6\%$, which remained below that of the single bottom cell. These numbers and results fit very well with the predictions from Equation (7) and (8). With the rough estimation of an average top-cell transparency of ≈30% (0% below, 65% above the bandgap, and assumed equal spectrum distribution between top and bottom cell), Equation (7) yields $\eta_{top,tandem} = 8.8\% \cdot 34.8/18.6 \cdot 0.3 = 5\%$, which in the sum with $\eta_{bottom,tandem} = 4.6\%$ gives the measured 9.6% tandem efficiency. However, the requirement of Equation (8), $\eta_{top,single} > 17.7\% \cdot (1–0.3) = 12\%$, is not met, and the tandem underperforms.

The $Cs_{0.09}FA_{0.77}MA_{0.14}Pb\ (I_{0.86}Br_{0.14})_3$ solar cell [11] was also integrated into a 2T tandem but in a monolithic configuration. This highlights an important point when evaluating top-cell transmission from literature: often, the measured solar cell stack does not or even cannot represent the configuration in the tandem, especially when electrical parameters of the single top cell shall also be measured. For precise optical analysis, a special stack replicating the exact layer configuration in the tandem device would be required. Therefore, in the monolithic perovskite/$Cu(In,Ga)Se_2$ tandem example presented here, it can only be stated that initially the individual bottom cell showed a short-circuit current density of 34.34 mA/cm$^2$ and an efficiency of 16.76%, while the current dropped to <18 mA/cm$^2$ in the tandem. However, as the single top cell had an efficiency exceeding 14%—significantly more than half that of the single bottom cell—it compensated for its slightly imperfect sub-bandgap transparency of on average 45%, allowing the tandem to outperform the single bottom cell and achieve an overall efficiency of 22.43%.

Figure 4b further presents transmission data for P3HT:PCBM [13] and $Sb_2S_3$ [14] solar cells, both deposited on a transparent back contact, however not measured in combination with a bottom cell yet. The organic P3HT:PCBM-based solar cell exhibits transmission values approaching 80% just below the bandgap but suffers a pronounced decline at longer wavelengths. A characteristic feature of organic absorber material is an often nonnegligible sub-bandgap transmission, which in some cases results in an average transparency of approximately 50% across the entire spectral range. However, this partial transparency does not necessarily facilitate efficient light distribution in a tandem configuration, highlighting the need for further optimization. Similarly, emerging materials such as $Sb_2S_3$ demonstrate significant potential for improving solar cell transmission.

Finally, Figure 4c illustrates the potential for optimizing the top-cell stack to enhance transparency. The initial $CuGaSe_2$ solar cell stack exhibited an average sub-bandgap transmission of ≈60% only. By systematically optimizing layer thicknesses to minimize parasitic absorption—not only within the $CuGaSe_2$ absorber but also in the contact layers—and to enable the top layers to act as an antireflection coating, transparency was improved by more than 20% absolute. As a result, the performance of a $Cu(In,Ga)Se_2$ bottom cell, when shaded by these two top-cell stacks, increased from $j_{sc} = 10.6$ mA/cm$^2$ and $\eta = 4.3\%$ to $j_{sc} = 15.7$ mA/cm$^2$ and $\eta = 6.3\%$. Given that the unshaded bottom cell came with a $j_{sc}$ of 38.9 mA/cm$^2$, achieving an efficient tandem would again require the top cell to surpass the bottom cell in efficiency—a remaining challenge for $CuGaSe_2$ [15]. Ultimately, both high-top-cell efficiency and high sub-bandgap transparency are essential for optimal tandem device performance.

It is important to note that the transparencies and efficiencies presented here are literature examples and may neither be generalized nor necessarily give the current record. Device performance is highly dependent on the choice of materials and fabrication conditions, and, as discussed, the exact device architecture and transmission should be identified for every specific case. Nonetheless, the visualized data provide valuable insights into realistic device behavior. Returning to our primary objective, we aim to establish a fundamental rule of thumb for determining when a tandem solar cell provides a net efficiency gain. This criterion is expressed by Equation (8), which states that the single top-cell efficiency must at least equal the bottom-cell efficiency scaled by the top cell's optical transmission losses. Additionally, Equation (7) highlights the direct link between the reduction of the top-cell efficiency in a bottom-cell-limited tandem and its own average transparency. This underscores the critical importance of high-top-cell transparency, a factor that is often underestimated in tandem solar cell design.

## 4 | Perspectives

To date, the most popular tandem configurations combine perovskite as the top-cell absorber with silicon or other bottom cells.

Perovskite materials have demonstrated the highest efficiencies for bandgaps around 1.7 eV, which are ideal for top absorbers. Efficiency records of 26.7% for single cell, 34.2% for perovskite/silicon, and 24.2% for perovskite/Cu(In,Ga)$Se_2$ tandem highlight their remarkable potential [16]. However, significant challenges related to stability and toxicity persist, driving the search for alternative wide-gap absorbers. Wide-gap chalcopyrites, such as Ga- or S-rich Cu(In,Ga)$(S,Se)_2$, are established candidates that have recently regained attention. In addition, materials like $Cu_2O$, $NaBiS_2$, $Sb_2(S,Se)_3$, and others are striving to enter the field. When exploring new materials for top cells, it is essential to carefully consider the requirements for transparency and efficiency outlined in Equation (7) and (8). As a general rule, achieving 50% efficiency relative to the bottom cell and 50% transmission for the top cell ensures that the tandem performs on par with the single bottom cell. However, to surpass the single bottom-cell performance, higher efficiency and transmission values are required. Sub-gap transparency remains a key challenge for many materials and complete solar cell structures, compare Figure 4, making it crucial for top-cell efficiencies to closely approach those of the bottom cell. The additional processing steps, material costs, and energy requirements are only justified if the tandem efficiency substantially exceeds that of the single bottom cell.

Enhancing top-cell transparency is a critical requirement that can be addressed through various approaches. While optimizing the absorber material to maximize above-bandgap absorption and minimize defect-related sub-gap losses is essential, other layers must also be considered. Contact layers, for instance, are a major source of transparency losses due to effects such as free charge carrier absorption. Balancing optical transparency and electrical conductivity is crucial, and studies have explored the variation of contact materials to mitigate losses [11]. Additionally, thin-film stacks exhibit complex light propagation, where layer thicknesses affect reflection and transmission. A more strategic design that exploits these optical principles offers further potential for improvement. Ref. [4] provides an exemplary breakdown of transparency losses in a $CuGaSe_2$ top cell, highlighting key loss mechanisms and their relative impact.

The remaining limitations caused by reduced transparency of the top cell can lead to decreased current in the bottom cell but, in the case of 2T configuration, even in the top cell itself. The approaches of light redistribution discussed in the following are particularly interesting for bottom-cell-limited tandems, as they help alleviate current-limiting constraints. One such approach, briefly mentioned earlier, involves reducing the thickness of the top cell to enhance light transmission. Studies have explored how varying the top absorber thickness affects top-cell absorption and spectral transmittance. The goal is to increase the bottom-cell current and the overall current of the 2T tandem system [17–19]. Additionally, current matching by solely adjusting the absorber thickness of the top and bottom cells has been discussed [20]. Further optimization of spectral distribution between the top and bottom cells can be achieved by introducing wavelength-selective intermediate reflectors. For example, photonic nanostructures can improve light management by reflecting low-energy light back and allowing high-energy light to pass through. Initial attempts at implementing such designs have been reported [21], though there is still room for improvement and optimization. Another important factor, not yet addressed in this discussion, is luminescent coupling between the top and bottom cell [22]. In cases of radiative recombination, above-bandgap light re-emitted by one cell can be absorbed by the adjacent cell. Re-emission from the bottom cell only partially benefits the absorption of the top cell, as this has a higher bandgap. Conversely, re-emission from the top cell can significantly enhance bottom-cell absorption and current. Finally, bifacial tandem solar cells, which utilize additional irradiation from the rear side, offer a promising strategy to increase bottom-cell current. Already today, 90% of silicon solar cells are bifacial [23]. Meanwhile, thin-film technologies inherently provide semitransparency, enabling their use as top cells in tandem structures but also creating opportunities for rear-illuminated bottom cells. While literature mostly addresses the adaptation ability of the top-cell bandgap [24–27], bifacial illumination is also able to compensate for imperfect top-cell transmission. Bifacial tandem cells, ideally including optical designs for improved attribution of the solar spectrum to the respective subcells, thus represent a promising future direction toward higher efficiencies.

To circumvent challenges caused by imperfect top-cell transmission, spectrum splitting offers a viable solution. This approach replaces transmission losses in tandem designs with the anticipated lower losses of spectrum-splitting optics. Placing the two solar cells adjacently or even separately can simplify manufacturing, reducing the challenges of combined growth to, at most, small-scale absorber fabrication. Spectrum splitting for photovoltaic applications has been demonstrated using technologies like micro-optics or waveguide-based systems [28, 29]. These systems can also incorporate elements such as refracting and diffracting objects and function as spectrum-splitting concentrators, in various configurations with receiving solar cells [30, 31]. Additionally, holographic lens systems have been proposed to capture both direct and diffuse light [32]. Spectrum splitting was furthermore exploited for light distribution between different applications, for example, photovoltaic and solar thermal fuel [33]. Also agrivoltaics benefits from spectrum-splitting concentrators, providing the dual advantage of optimizing plant illumination while directing the spectrum unsuitable for crop growth to photovoltaic cells [34].

Given that multijunction solar cells generally exhibit low material efficiency [35], combining them with light concentration is a promising strategy for maximizing efficiency gains. Micro- or millimeter-scale concentrator cells are preferred over macroscopic counterparts due to their improved heat dissipation, compact size, and ease of tracking [36] (an example for simplified tracking is given in Ref. [37]). Medium concentration factors can be advantageous as they mitigate challenges related to precision and miniaturization while capturing most of the efficiency gain. The logarithmic dependence of efficiency on light intensity ensures substantial improvements at lower concentrations, with diminishing returns at higher levels. In addition, bifacial solar cells can harness diffuse light alongside concentrated direct light, offering further efficiency improvements. Bifacial tandem concentrator solar cells are, therefore, also a compelling option. Given the variations in light intensity, a 3T tandem configuration is advantageous for such designs to overcome current-matching constraints. Figure 5 illustrates a spectrum-splitting bifacial 3T tandem concentrator solar cell envisioned for the future.

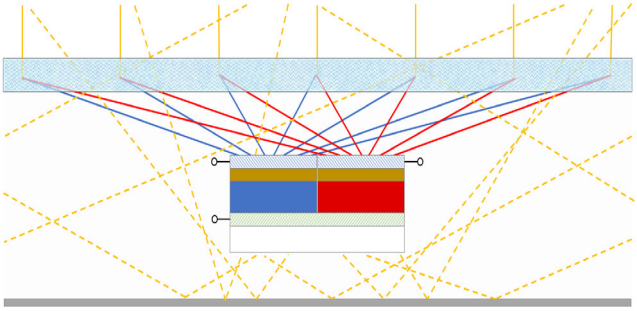

**FIGURE 5** | Adjacent wide (blue) and low (red) bandgap solar cell with common transparent back (green shaded) but separated front (blue shaded) contact for 3T tandem configuration under spectrum-splitting concentrator optics (light blue) and with rear reflector (gray) for bifacial illumination and combined exploitation of direct (solid lines) and diffuse (dashed lines) light (scale relations adapted for improved visibility, supporting structure not shown).

The final efficiency achievable with this configuration strongly depends on the irradiation conditions, particularly the fraction of diffuse light which determines the bifacial gain. The latter is further influenced by the solar cells' bifaciality, defined as the rear-to-front illumination performance ratio. Additionally, in the current configuration, rear illumination is neither concentrated nor spectrally split, presenting opportunities to further optimize the optical design—an essential step toward maximizing efficiency in tandem devices.


### Acknowledgments

T.H. Witte-Nguy is acknowledged for reference setting and formatting and M. Misch for optimizing the drawing of the TOC figure. The author acknowledges support from the Open Access Publication Fund of the University of Duisburg-Essen.

Open Access funding enabled and organized by Projekt DEAL.


### Conflicts of Interest

The author declares no conflicts of interest.

### Data Availability Statement

The author has nothing to report.

### References


1. M. Schmid, "Optik der $CuGaSe_2$-Solarzelle für Hocheffiziente Tandemkonzepte," (*PhD thesis*, Freie Universität Berlin, 2009).

2. A. Martí and G. L. Araújo, "Limiting Efficiencies for Photovoltaic Energy Conversion in Multigap Systems," *Solar Energy Materials and Solar Cells* 43 (1996): 203.

3. T. J. Coutts, J. S. Ward, D. L. Young, K. A. Emery, T. A. Gessert, and R. Noufi, "Critical Issues in the Design of Polycrystalline, Thin-Film Tandem Solar Cells," *Progress in Photovoltaics: Research and Applications* 11 (2003): 359.

4. M. Schmid, R. Klenk, and M. C. Lux-Steiner, "Quantitative Analysis of Cell Transparency and Its Implications for the Design of Chalcopyrite-Based Tandems," *Solar Energy Materials and Solar Cells* 93 (2009): 874–878.

5. M. van Eerden, M. Jaysankar, A. Hadipour, et al., "Optical Analysis of Planar Multicrystalline Perovskite Solar Cells," *Advanced Optical Materials* 5 (2017): 1700151.

6. A. Bojar, D. Micha, M. Giteau, et al., "Optical Simulations and Optimization of Perovskite/CI(G)S Tandem Solar Cells Using the Transfer Matrix Method," *Journal of Physics: Energy* 5 (2023): 035001.

7. I. M. Peters, S. Sofia, J. Mailoa, and T. Buonassisi, "Techno-Economic Analysis of Tandem Photovoltaic Systems," *RSC Advances* 6 (2016): 66911.

8. K. Alberi, J. J. Berry, J. J. Cordell, et al., "A Roadmap for Tandem Photovoltaics," *Joule* 8 (2024): 658.

9. E. L. Warren, W. E. McMahon, M. Rienäcker, et al., "A Taxonomy for Three-Terminal Tandem Solar Cells," *ACS Energy Letters* 5 (2020): 1233.

10. Z. Yu, M. Leilaeioun, and Z. Holman, "Selecting Tandem Partners for Silicon Solar Cells," *Nature Energy* 1 (2016): 16137.

11. Q. Han, Y.-T. Hsieh, L. Meng, et al., "High-Performance Perovskite/$Cu(In,Ga)Se_2$ Monolithic Tandem Solar Cells," *Science* 361 (2018): 904.

12. N. Barreau, L. Choubrac, F. Pineau, et al., Full Chalcopyrite Tandem Devices: Can We Hope?, in IEEE 52nd PVSC, Seattle, USA, June, 2024.

13. D. J. Lee, D. K. Heo, C. Yun, Y. H. Kim, and M. H. Kang, "Solution-Processed Semitransparent Inverted Organic Solar Cells from a Transparent Conductive Polymer Electrode," *ECS Journal of Solid State Science and Technology* 8 (2019): Q32.

14. S.-J. Lee, S.-J. Sung, K.-J. Yang, et al., "Approach to Transparent Photovoltaics Based on Wide Band Gap $Sb_2S_3$ Absorber Layers and Optics-Based Device Optimization," *ACS Applied Energy Materials* 3 (2020): 12644.

15. M. Schmid, R. Caballero, R. Klenk, et al., "Experimental Verification of Optically Optimized $CuGaSe_2$ Top Cell for Improving Chalcopyrite Tandems," *EPJ Photovoltaics* 1 (2010): 10601.

16. M. A. Green, E. D. Dunlop, M. Yoshita, et al., "Solar Cell Efficiency Tables (version 64)," *Progress in Photovoltaics: Research and Applications* 32 (2024): 425.

17. S. R. Kurtz, P. Faine, and J. M. Olson, "Modeling of Two-Junction, Series-Connected Tandem Solar Cells Using Top-Cell Thickness as an Adjustable Parameter," *Journal of Applied Physics* 68 (1990): 1890.

18. M. Schmid, J. Krč, R. Klenk, M. Topič, and M. C. Lux-Steiner, "Optical Modeling of Chalcopyrite-Based Tandems considering Realistic Layer Properties," *Applied Physics Letters* 94 (2009): 053507–053501.

19. I. Almansouri, A. Ho-Baillie, S. P. Bremner, and M. A. Green, "Supercharging Silicon Solar Cell Performance by Means of Multijunction Concept," *IEEE Journal of Photovoltaics* 5 (2015): 968.

20. S. Yadav, M. A. Kareem, H. K. Kodali, et al., "Optoelectronic Modeling of All-Perovskite Tandem Solar Cells with Design Rules to Achieve >30% Efficiency," *Solar Energy Materials and Solar Cells* 242 (2022): 111780.

21. V. Neder, S. W. Tabernig, and A. Polman, "Detailed-Balance Efficiency Limits of Two-Terminal Perovskite/Silicon Tandem Solar Cells with Planar and Lambertian Spectral Splitters," *Journal of Photonics for Energy* 12 (2022): 015502.

22. A. R. Bowman, F. Lang, Y.-H. Chiang, et al., "Relaxed Current Matching Requirements in Highly Luminescent Perovskite Tandem Solar Cells and Their Fundamental Efficiency Limits," *ACS Energy Letters* 6 (2021): 612.

23. M. Fischer, M. Woodhouse, and P. Baliozian, "International Technology Roadmap for Photovoltaic (ITRPV), 2022 Results," 15th ed. 2024, https://vdma.org/international-technology-roadmap-photovoltaic.

24. J. Chantana, Y. Kawano, T. Nishimura, A. Mavlonov, and T. Minemoto, "Optimized Bandgaps of Top and Bottom Subcells for Bifacial Two-Terminal Tandem Solar Cells under Different Back Irradiances," *Solar Energy* 220 (2021): 163.

25. M. De Bastiani, A. J. Mirabelli, Y. Hou, et al., "Efficient Bifacial Monolithic Perovskite/Silicon Tandem Solar Cells via Bandgap Engineering," *Nature Energy* 6 (2021): 167.

26. K. Jäger, P. Tillmann, E. A. Katz, and C. Becker, "Perovskite/Silicon Tandem Solar Cells: Effect of Luminescent Coupling and Bifaciality," *Solar RRL* 5 (2021): 2000628.

27. J. Tang, J. Xue, H. Xu, et al., "Power Generation Density Boost of Bifacial Tandem Solar Cells Revealed by High Throughput Optoelectrical Modelling," *Energy & Environmental Science* 17 (2024): 6068.

28. D. Li, J. Michel, J. Hu, and T. Gu, "Compact Spectrum Splitter for Laterally Arrayed Multi-Junction Concentrator Photovoltaic Modules," *Optics Letters* 44 (2019): 3274.

29. T. Veeken, J. van de Groep, W. Knight, and M. A., Waveguide-Based Spectrum-Splitting Concept for Parallel-Stacked Tandem Solar Cells (conference Presentation), SPIE Photonics Europe, April, 2018.

30. C. Maragliano, M. Chiesa, and M. Stefancich, "Point-Focus Spectral Splitting Solar Concentrator for Multiple Cells Concentrating Photovoltaic System," *Journal of Optics* 17 (2015): 105901.

31. A. Elikkottil, M. H. Tahersima, S. Gupta, V. J. Sorger, and B. Pesala, "Silicon Nitride Grating Based Planar Spectral Splitting Concentrator for NIR Light Harvesting," *Optics Express* 28 (2020): 21474.

32. S. D. Vorndran, B. Chrysler, B. Wheelwright, R. Angel, Z. Holman, and R. Kostuk, "Off-Axis Holographic Lens Spectrum-Splitting Photovoltaic System for Direct and Diffuse Solar Energy Conversion," *Applied Optics* 55 (2016): 7522.

33. W. Qu, H. Hong, and H. Jin, "A Spectral Splitting Solar Concentrator for Cascading Solar Energy Utilization by Integrating Photovoltaics and Solar Thermal Fuel," *Applied Energy* 248 (2019): 162.

34. Z. Zhang, F. Zhang, W. Zhang, et al., "Spectral-Splitting Concentrator Agrivoltaics for Higher Hybrid Solar Energy Conversion Efficiency," *Energy Conversion and Management* 276 (2023): 116567.

35. M. Schmid, "Revisiting the Definition of Solar Cell Generations," *Advanced Optical Materials* 11 (2023): 2300697.

36. M. Alves, A. Pérez-Rodríguez, P. J. Dale, C. Domínguez, and S. Sadewasser, "Thin-Film Micro-Concentrator Solar Cells," *Journal of Physics: Energy* 2 (2019): 012001.

37. J. M. Hallas, K. A. Baker, J. H. Karp, E. J. Tremblay, and J. E. Ford, "Two-Axis Solar Tracking Accomplished through Small Lateral Translations," *Applied Optics* 51 (2012): 6117.